Sublimation as a landform-shaping process on Pluto

Jeffrey M. Moore [a,*], Alan D. Howard [b], Orkan M. Umurhan [a], Oliver L. White [a],
Paul M. Schenk [c], Ross A. Beyer [d,a], William B. McKinnon [e], John R. Spencer [f],
Will M. Grundy [g], Tod R. Lauer [h], Francis Nimmo [i], Leslie A. Young [f], S. Alan Stern [f],
Harold A. Weaver [j], Cathy B. Olkin [f], Kimberly Ennico [a], the New Horizons Science Team

[a] NASA Ames Research Center, Moffett Field, CA, 94035, USA
[b] Dept. Environmental Sciences, University of Virginia, Charlottesville, VA 22904, USA
[c] Lunar and Planetary Institute, Houston, TX 77058, USA
[d] The SETI Institute, Mountain View, CA 94043, USA
[e] Dept. Earth and Planetary Sciences, Washington University, St. Louis, MO 63130, USA
[f] Southwest Research Institute, Boulder, CO 80302, USA
[g] Lowell Observatory, Flagstaff, AZ 86001, USA
[h] National Optical Astronomy Observatory, Tucson, AZ 85719, USA
[i] University of California, Santa Cruz, CA 95064, USA
[j] Johns Hopkins University, Applied Physics Laboratory, Laurel, MD 20723, USA

ARTICLE INFO

ABSTRACT

Fields of pits, both large and small, in Tombaugh Regio (Sputnik Planitia, and the Pitted Uplands to the east), and along the scarp of Piri Rupes, are examples of landscapes on Pluto where we conclude that sublimation drives their formation and evolution. Our heuristic modeling closely mimics the form, spacing, and arrangement of a variety of Tombaugh Regio's pits. Pluto's sublimation modified landforms appear to require a significant role for (diffusive) mass wasting as suggested by our modeling. In our models, the temporal evolution of pitted surfaces is such that initially lots of time passes with little happening, then eventually, very rapid development of relief and rapid sublimation. Small pits on Sputnik Planitia are consistent with their formation in N_2-dominated materials. As N_2-ice readily flows, some other "stiffer" volatile ice may play a role in supporting the relief of sublimation degraded landforms that exhibit several hundred meters of relief. A strong candidate is CH_4, which is spectroscopically observed to be associated with these features, but the current state of rheological knowledge for CH_4 ice at Pluto conditions is insufficient for a firm assessment.

Published by Elsevier Inc.

1. Introduction

Several icy-world surfaces in the solar system exhibit sublimation-driven landform modification expressed through mass wasting, erosion, and, in some cases, local recondensation of volatiles (Moore et al., 1996, 1999; Mangold, 2011). Erosion from mass wasting can utilize internal disaggregation of the relief-forming material either through decomposition of the bedrock or through the loss (or deteriorating alteration) of its cohesive matrix or cement. The sublimation of a volatile ice either as a bedrock or a cohesive matrix can fulfill this role. To give several examples, Callisto's landscape exhibits widespread erosion from sublimation erosion of the volatile matrix of the relief supporting material.

Of the two ices present (H_2O and CO_2), CO_2 is thought to be the major sublimating agent. The disaggregation of relief-supporting material (composed of the two ices plus abundant fine grained silicate particles) caused slopes to retreat and collapse, resulting in smooth, undulating, low albedo plains composed of lag deposits, with isolated high albedo pinnacles composed of the less volatile H_2O ice perched on local summits (such as the remnants of crater rims), which serve as cold traps for re-precipitating of H_2O on Callisto (Howard and Moore, 2008; White et al., 2015). Erosion is suppressed on lower lag covered slopes and ridges are crowned with a high albedo and insulating cap of reprecipitated H_2O ice. The evolution of the "honeycomb" topography of Hyperion has been explained as a product of impact cratering with reduced proximal ejecta redeposition and loss of bedrock strength by sublimation coupled with diffusive mass wasting (Howard et al., 2012). On the Martian North Polar Cap the landscape is shaped by a combination of ice sublimation and deposition with the

addition of the role of wind erosion (Howard, 1978, 2000). Also on Mars sublimation produces periglacial scalloped pits (Dundas et al., 2015), distinctive pitting in the south polar CO_2 cap (Byrne and Ingersoll, 2003), and "spiders" produced by a solid-state greenhouse producing CO_2 outgassing (Kieffer, 2007; Piqueux and Christensen, 2008). Penitentes on terrestrial equatorial ice fields are a consequence of sublimation, not melting (Matthes, 1934; Lliboutry, 1954; Amstutz, 1958). Sublimation-driven mass wasting was anticipated on Pluto prior to the encounter (Moore et al., 2015).

Here we report on several landscapes on Pluto we interpret to be formed or at least heavily modified by sublimation erosion. The instruments aboard the *New Horizons* spacecraft used to collect data presented in this paper were the medium-resolution color wide-angle "push-broom" camera (MVIC- Multispectral Visible Imaging Camera), the high resolution framing panchromatic camera (LORRI- LOng Range Reconnaissance Imager), and the 256 channel imaging spectrometer (LEISA -Linear Etalon Imaging Spectral Array). Specifications and other details about these instruments are available elsewhere (e.g., Reuter et al., 2008; Cheng et al., 2008). We discuss evolution scenarios for these landscapes including modeling the possible evolution of some of these landforms utilizing a landform evolution model developed by Howard (Howard, 1994, 2007; Forsberg-Taylor et al., 2004; Howard and Moore, 2008; Barnhart et al., 2009; Howard et al., 2012, 2016).

2. Observations, inferences, and speculation

Several terrains within Pluto's cratered uplands are probably shaped, wholly or in part, by sublimation erosion and/or volatile redistribution. The tenuous atmosphere of Pluto is dominated by N_2 sublimated from surface ices. Perhaps the easiest sublimation features to recognize on Pluto are the rimless pits dotting much of Sputnik Planitia (Moore et al., 2016), and we examine these pits first. (Note that all place names used in this paper are informal.)

2.1. Sputnik Planitia pits and chains

Observations: Incipient textures that appear to transition into full scale pitting occur almost everywhere across the surface of the predominantly nitrogen ice plains of Sputnik Planitia (Stern et al., 2015; Moore et al., 2016) (Fig. 1). The pits exhibit variations in size, width/depth ratio, density, aspect ratio and alignment across the Planitia (Figs. 2–5), and generally become larger and tend to be more organized (into chains) progressively southward (White et al., 2016). In the cellular plains of central and northern Sputnik Planitia (Stern et al., 2015; Moore et al., 2016), pitting is finely textured (Fig. 3). Discrete shoulder-to-shoulder pits (individual pits a few hundred of meters across) are recognizable only in images acquired at ∼100 m/pixel or better (Fig. 4a) at ∼20–25°N. The pits in Fig. 4a are roughly equidimensional and do not form chains. Elsewhere in the cellular plains, small shoulder-to-shoulder pits are elongate and begin to form chains (Figs. 2, 4b and e). Preliminary photoclinometric measurements indicate the vast majority of pits on the N_2-ice dominated Sputnik Planitia (Moore et al., 2016) are only a few tens of meters deep, which is consistent with the low viscosity of N_2-ice, which quickly diffuses deep depressions (see Properties section).

The plains of southern Sputnik Planitia display pits that reach larger sizes (typically a few kilometers across) than those in the cellular plains, and which organize into fields of often-aligned pit chains that appear especially well developed as seen in high-resolution images (Fig. 3). Pits and pit chains are observed to occur in isolation, with smooth plains separating them from their neighbors (Fig. 4d and f), and the orientations of the pit chains vary across the Planitia (Fig. 3). Larger elongated pits (typically 2–3 km
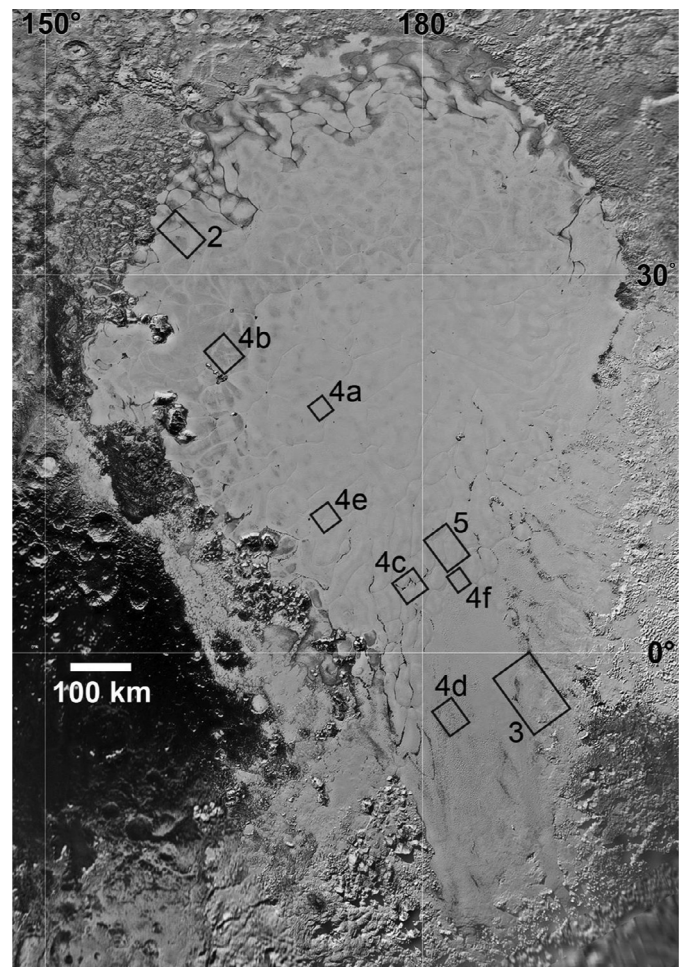
Fig. 1. Location-map of pits and other sublimation related figures shown elsewhere in the text on a base map of Sputnik Planitia. All place names used in the paper are informal (see map in Moore et al. (2016), Figure S1 in supplemental online materials for locations of named features).

long and 0.5 km wide) locally organize into complex, swirling "fingerprint" patterns colloquially referred to as *Sputnik Bacilli* (Figs. 3 and 4d).

The scale and morphology of pits often varies systematically with position relative to the large convective cells on Sputnik Planitia, which have dimensions of tens of kilometers (Stern et al., 2015; Moore et al., 2016; McKinnon et al., 2016). Often pitting is shallow to sparse in cell centers, dense and deep near the convective cell edges, and again shallow, and often sparse along the convective cell margins (Fig. 5, White et al., 2016). In other locations the pitting is shallow and sparse, with the shallowest pitting occurring as indistinct, rounded depressions. (Fig. 4f).

Inferences and Speculations: Possible mechanisms forming the pitted terrain include sublimation, wind transport, or wind enhanced sublimation erosion, and perhaps ground collapse. The ∼10 μbar surface pressure of the current atmosphere is unlikely to have the capacity to move particles, presumably in saltation, that could abrade or deflate the landscape to form pits (e.g., Chyba and Sagan, 1990; Moore et al., 2015). There are no unambiguous aeolian landforms (e.g., dunes) observed on Pluto, which is consistent with either a lack of sand sized particles, and/or surface winds, either in the present or past, capable of transporting them. A persistent directional wind, however, could perhaps enhance sublimation along wind-facing scarps causing elongation of pits. Strings of pits formed by ground collapse are seen on such worlds as Mars
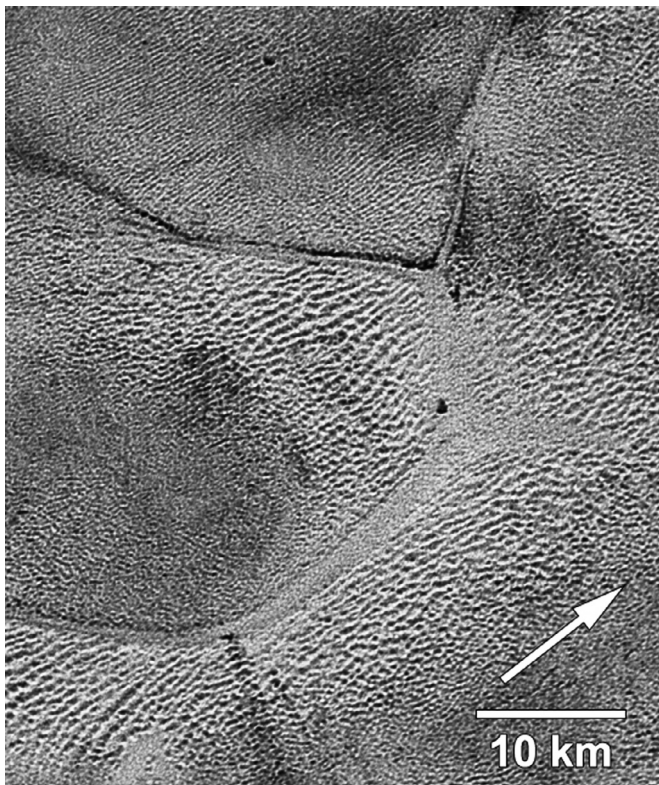
Fig. 2. Densely-pitted surface of Sputnik Planitia showing pits of differing scales. Intersecting linear bands 1–2 km wide are boundaries of convection cells. Image is taken from 79 m/pixel LORRI coverage of the PELR_P_MVIC_LORRI_CA observation, centered at 160.88°E, 33.51°N. Arrow points North. Illumination from above.
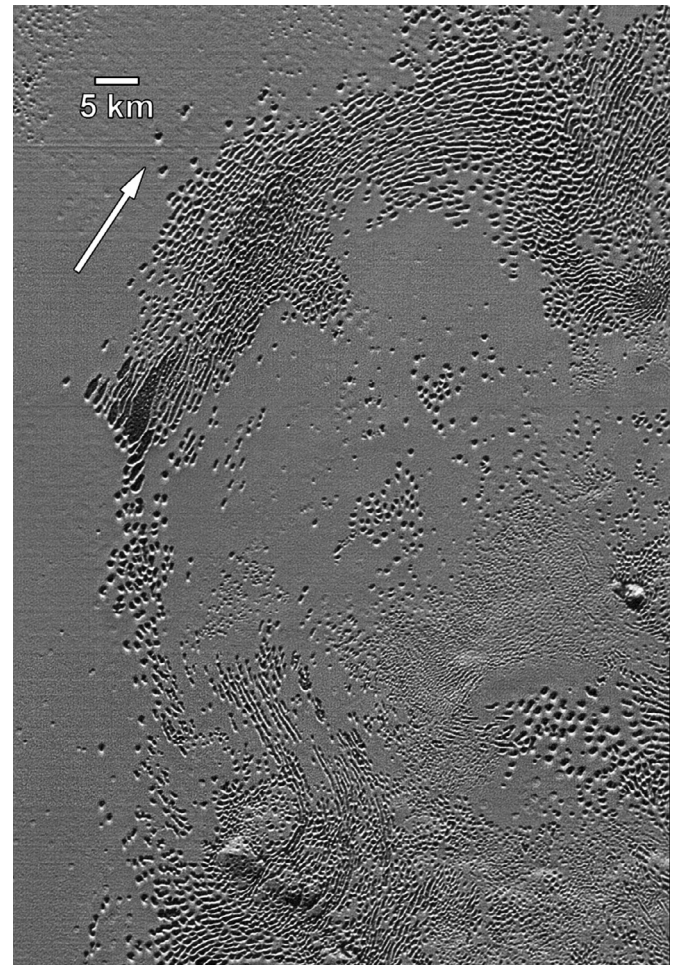
Fig. 3. Sparse, deep pitting showing elongated, parallel pits informally referred to as "bacilli". Image is taken from 79 m/pixel LORRI coverage of the PELR_P_MVIC_LORRI_CA observation, centered at 188.60°E, 3.43°S. Arrow points North. Illumination from above.

and Phobos, however, these collapse pits in these strings do not normally exhibit regular spacing with (lateral or parallel-running) neighboring strings of collapse pits, whereas the Pluto pits do. Also individual pits in collapse pit chains often exhibit significant variation in length from pit to pit, unlike the pits on Sputnik Planitia.

We conclude that sublimation is the primary process forming the Sputnik Planitia pitting. The sublimation pitting on Sputnik Planita appears to have developed into ices that are relatively free of insoluble residues with different albedo (e.g., dust, tholins). Impure ices in snow and ice collect particles on the divides of sublimation pits as they erode, forming the distinct dark crests on terrestrial suncups (Rhodes et al., 1987). The floors of some deep pits on Sputnik Planitia, however, are distinctly dark and relatively flat (Figs. 3 and 4c). These pits are seen in the marginal areas of Sputnik Planitia, where the nitrogen ice is expected to be thinner than in the center. We speculate that sublimation has exposed a distinct, dark albedo layer (tholins?) with reduced susceptibility to sublimation. In particular, extensive fields of dark-bottomed pits are seen in western Sputnik Planitia directly adjacent to the dark highlands of Cthulhu Regio, and the floors may be exposing such highlands terrain appear to be covered by relatively shallow ice here.

However, this is likely not the case for dark-bottomed pits seen within the cellular plains closer to the center of Sputnik Planitia, where the nitrogen ice may reach kilometers thick, based on considerations of solid-state convection here (Moore et al., 2016; McKinnon et al., 2016) – too thick for sublimation to deepen pits to the base of the nitrogen ice. Dark-bottomed pits here invariably concentrate in the troughs that mark the cell boundaries (e.g. Fig. 4c). This distribution raises the possibility that the dark material here originates from atmospheric transport (either fallout or through saltation) and becomes trapped within these troughs. The low albedo may initially cause preferential heating of the ice un-

derneath it, and therefore increased sublimation and pit growth rates, at least until the dark floor material is thick enough to provide an insulating lag, or else further pit growth is suppressed by inward flow of soft N_2-ice.

The fingerprint patterns (Figs. 3 and 4d) probably develop in response to non-homogenous, anisotropic substrate properties, such as compositional or textural (grain size or grain orientation) layering, fractures or crevasses. Some of these fingerprint patterns are associated with inferred active glacial flows, and are elongated along flow margins, supporting the notion that the pits nucleated from aligned structures in the surficial ices. Sublimation-induced pitting appears to compete with diffusive flow of the near-surface ices, which tends to smoothen the surface. N_2-rich ices have very low viscosity (Eluszkiewicz and Stevenson,1990; Yamashita, et al., 2010; see "Properties" section), and convection in these ices forms the large convection cells affecting most of Sputnik Planitia (Stern et al., 2015; Moore et al., 2016; McKinnon et al., 2016; Trowbridge et al., 2016). The smooth surface of parts of Sputnik Planitia, locally mottled with sparse, rounded, very shallow pitting suggests they may have been deeper pits presently undergoing degradation (healing) by lateral ice flow. We present a preliminary model below (see "Modeling" section) that explores the competitive interaction between formation and deepening of pits due to sublimation versus mass flow that tends to smooth the surface.

Fig. 4. Variations in pit morphology on Sputnik Planitia. 5 km scale bars. North is approximate 45° clockwise. See text for details. (a) and (f) are taken from 79 m/pixel LORRI coverage of the PELR_P_MVIC_LORRI_CA observation. (b) through (e) are taken from 125 m/pixel LORRI coverage of the PELR_P_MPAN_1 observation. Image centers: (a) 172.11°E, 19.76 °N; (b) 164.26°E, 23.71°N; (c) 179.10°E, 5.38°N; (d) 182.04°E, 4.93°S; (e) 172.32°E, 10.86°N; (f) 183.03°E, 5.71°N. Illumination from above.

2.2. East Tombaugh Regio pitted uplands

Observations: As was reported in Moore et al. (2016), a distinctive, high-albedo landscape of intricate pits and smooth plains borders and extends about 500 km eastward from Sputnik Planitia, and forms most of the right "ventricle" of Tombaugh Regio (roughly centered 15°N, 200°E) (Fig. 6). The dominant feature of this landscape are the pits, most of which are around 3–10 km across, but some exceed 25 km, locally intersecting to form long, structurally-controlled troughs. Based upon DEM derived topography, the deepest pits are 2 or more km deep. The summits (or crests) of the pit septa collectively define a broadly undulating, though heavily modified, plateau or upland surface 2 to 4 km above Sputnik Planitia. The sidewalls of the pits are steep (~30°) and can support relief greater than a km, indicating that the material composing the pit septa is rigid, ruling out N_2 or CO-ice as a major component. The densely-pitted terrain has a strong CH_4 signature (Grundy et al., 2016), which may constitute the rigid framework. Interspersed within the pitted uplands are patches of smooth plains with a strong N_2-ice spectral signature (Grundy et al., 2016) forming nearly level expanses up to 50 km across and
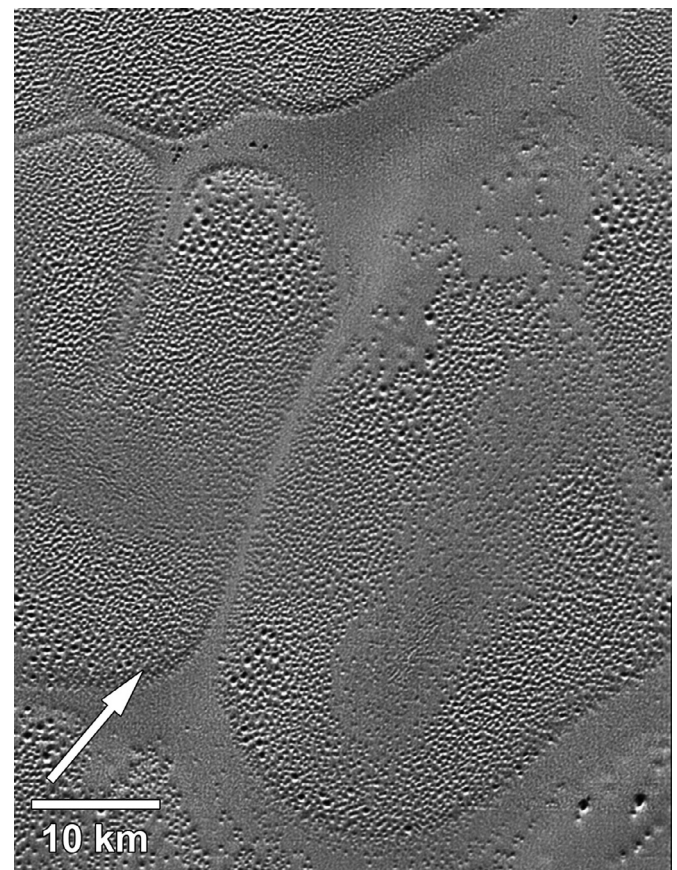
Fig. 5. The overprinting of sublimation pitting on the large convective cells (scale tens of kilometers) often exhibits a distinctive pattern in which pitting is shallow to sparse in cell centers, dense and deep near the convective cell edges, and again shallow, and often sparse along the convective cell margins. This pattern could be due to (1) systematic surface age variation; (2) thermal effects due to convective cell motion; or (3) compositional effects. Image is taken from 79 m/pixel LORRI coverage of the PELR_P_MVIC_LORRI_CA observation, centered at 181.81°E, 8.42°N. Illumination from above.

occurring at various elevations at relative low points in the pitted terrain.

Inferences and Speculations: The pitted terrain may be remnants of a formerly continuous deposit degraded either by sublimation, forming features analogous to terrestrial penitentes and sun-cups (but much larger), or through undermining and collapse, possibly through basal melting. It is possible that relief on the pit crests may be increased by condensation of sublimated methane in a manner similar to pinnacle formation on Callisto (Moore et al., 1999; Howard and Moore, 2008; White et al., 2015). In this study we will consider the role of sublimation in the formation of the pitted uplands as a possible larger manifestation of our modeling of the smaller pits on Sputnik Planitia.

2.3. Piri Rupes scarp retreat

Observations: Centered around ~30°N, 105°W is a scarp-enclosed basin informally named Piri Planitia, which contains mottled plains (Fig. 7). The basin is elongate roughly N-S, ~500 km along this dimension and up to ~260 km at its widest, near where graben and scarps of Inanna and Dumuzi Fossae enter the basin from the west Fig. 7b). The basin is roughly split into two general levels on either side of the Inanna and Dumuzi Fossae tectonic zone, with the southern portion of Piri Planitia being generally lower and better defined. This southern portion of Piri Planitia is relatively uncratered compared with most of the terrains that
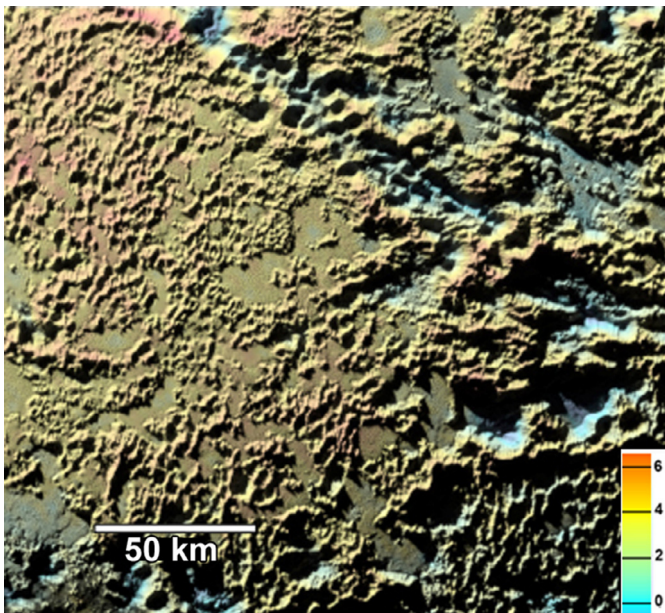
Fig. 6. Landforms of the East Tombaugh Region Pitted Upland. Regions of dense pits 3–10 km wavelength are interspersed with smoother terrain, likely rich in N_2 and CO-ices. The smooth terrain displays a pitted surface similar in scale that on Sputnik Planitia. The larger pits must have a rigid component, likely methane ice, given their relief of several hundred meters to 2 or more km. In places pits appear to coalesce with crestlines aligned in an NE-SW orientation, similar to the simulation shown in Fig. 14. Part of MVIC image PEMV_01_P_MVIC_LORRI_CA centered at 203.50°E, 0.33°S. North to top. Color elevation scale in lower right is in km. Illumination from upper left.

surround it. Both the southern and northern portion of Piri Planitia are hilly and rough at the scale of the photogrammetrically derived Digital Elevation Models (DEMs), which have a resolution of not better than 415 m horizontal and 150 m vertical (Fig. 7a and 7c). The northern portion of Piri Planitia is the rougher, contains more craters, and has less well-defined and lower relief bounding scarps. Beyond (north) of these scarps the land transitions to the fretted terrain of Venera Terra.

The bounding scarps of Piri Planitia are most pronounced along the lower, southern portion of the basin. These scarps (Piri Rupes) break up into isolated mesas in several places. DEM derived elevations indicate that local relief on the scarps typically range from ~600 m to ~1 km. The scarps display sharply pointed projections into the basin interspaced by embayments of plains into the plateaus. Where seen at best resolution (~230 m/pixel LORRI imaging) a portion of the scarp, at least at this location, exhibits prominent pitting along its crests, somewhat resembling the East Tombaugh uplands (Fig. 8). The land south of Piri Planitia (~20°N and southward) is divided into a smooth plateau region (eastern Vega Terra) west of roughly 110°E, and rough and heavily cratered uplands terrain to the east.

Inferences and Speculations: In places the scarps are shown in the DEMs to stand higher than the plateau surfaces beyond Piri Planitia, implying either material has been preferentially deposited on the scarp crests, or that the scarps incorporate segments of older high standing topography such a portions of crater rims. Perhaps the observed pitting along the scarp grows to undermine presumably less volatile materials, which might, in turn, induce scarp retreat. The presentation of the scarps, with their embayments of plains and sharp projections of headlands are characteristics of scarps that have formed though erosional retreat, also known as decrescence (e.g., Lange, 1959).

The plateau terrains to the south immediately above the scarp show a strong CH_4 signature while the plains below do not

(Fig. 7d). We speculate that CH_4 sublimation may be causing the plateau material to decay along the face of the scarps, driving the scarp retreat. The mottled plains unit of Piri Planitia below the scarps exhibits a H_2O signature, which may be from the involatile debris littering the plain following scarp retreat. The heights of the Piri Rupes scarps are such that the material supporting the scarps may require more mechanical strength than that of pure CH_4 ice. H_2O ice is both refractory and can support several km of relief in the Pluto surface environment. Thus there are at least two possibilities. One is that CH_4 occurs as layers with presumably H_2O ice above it as a cap rock. The loss of CH_4 to sublimation along the scarp faces undermines the cap rock and the scarps retreat, leaving H_2O ice blocks littering the plains following retreat. Alternatively a mixture of H_2O and CH_4 ices, in which the CH_4 ice is the cementing matrix, holding up the scarps. When the CH_4 sublimates once exposed, the cliff faces disaggregate and the scarps retreat, also leaving a H_2O detritus behind on the plains. Either case presupposes that H_2O ice is a relatively minor component and, once liberated, mass wastes away from the scarps rather than burying them.

2.4. Other potentially sublimation modified terrains

As was discussed in Moore et al. (2016), sublimation erosion may have played a significant role in the development of the Bladed terrain of Tartarus Dorsa (centered roughly 20°N, 225°E), Fretted terrain of southern Venera Terra (centered roughly 50°N, 100°E), and the large deep pits of the Arctic Eroded Mantle terrain (centered roughly 60°N, 210°E) (See Figs 3, S5, and S6 in Moore et al., 2016). These landscapes, however, very probably have histories that are sufficiently complex that they should, and will, be treated separately in forthcoming reports.

3. Some properties of ices at Pluto

Molecular nitrogen, CH_4, CO, and H_2O ices are all observed spectroscopically on Pluto (Grundy et al., 2016). Nitrogen, CH_4 and CO are solid at Pluto's surface temperatures of ~40 K (Fig. 9). N_2 and CO are much less viscous than water ice at ~270 K, and thus flow readily under the low stresses on Pluto (see Umurhan et al., 2016, this issue). CH_4 is relatively less volatile and may be significantly more rigid than N_2 and CO. Nitrogen ice is denser than water ice at 40 K. Methane ice is the least dense of all these ices where $\rho = 450$ kg/m^3, whereas the other ices have densities closer to 1000 kg/m^3, the triple point of CH_4 occurs at ~91 K and at about 0.1 bars (Fray and Schmidt, 2009). Water ice is probably the "bedrock" at Pluto, supporting steep mountains up to 4 km high.

In the following discussion we examine the potential for pure methane ice to mechanically support structures like those typical of the pitted uplands, for example. The rheology of methane, which is poorly known under Pluto's surface conditions, figures directly into this question. We here present the results of calculations pertaining to the mechanical lifetime of structures ("mounds") comprised strictly of methane based on published rheological studies of methane. We summarize our results here while a detailed explanation can be found in Appendix.

We consider methane mounds of vertical scale H and horizontal scale L resting on a flat bedrock of infinite strength, where the sloping grade θ is related to these dimensions by $\tan\theta \approx \theta = H/L$. Structures comprised of a given material and basal tangential stresses will exhibit a characteristic strain rate $\dot{\epsilon}$, from which follows a corresponding e-folding relaxation timescale of the structure, τ, given from $\tau^{-1} \sim \dot{\epsilon} H/L$.

There are three known published studies of solid methane's rheology covering the conditions of Pluto's surface temperatures and shallow subsurface pressures (see Appendix). The first
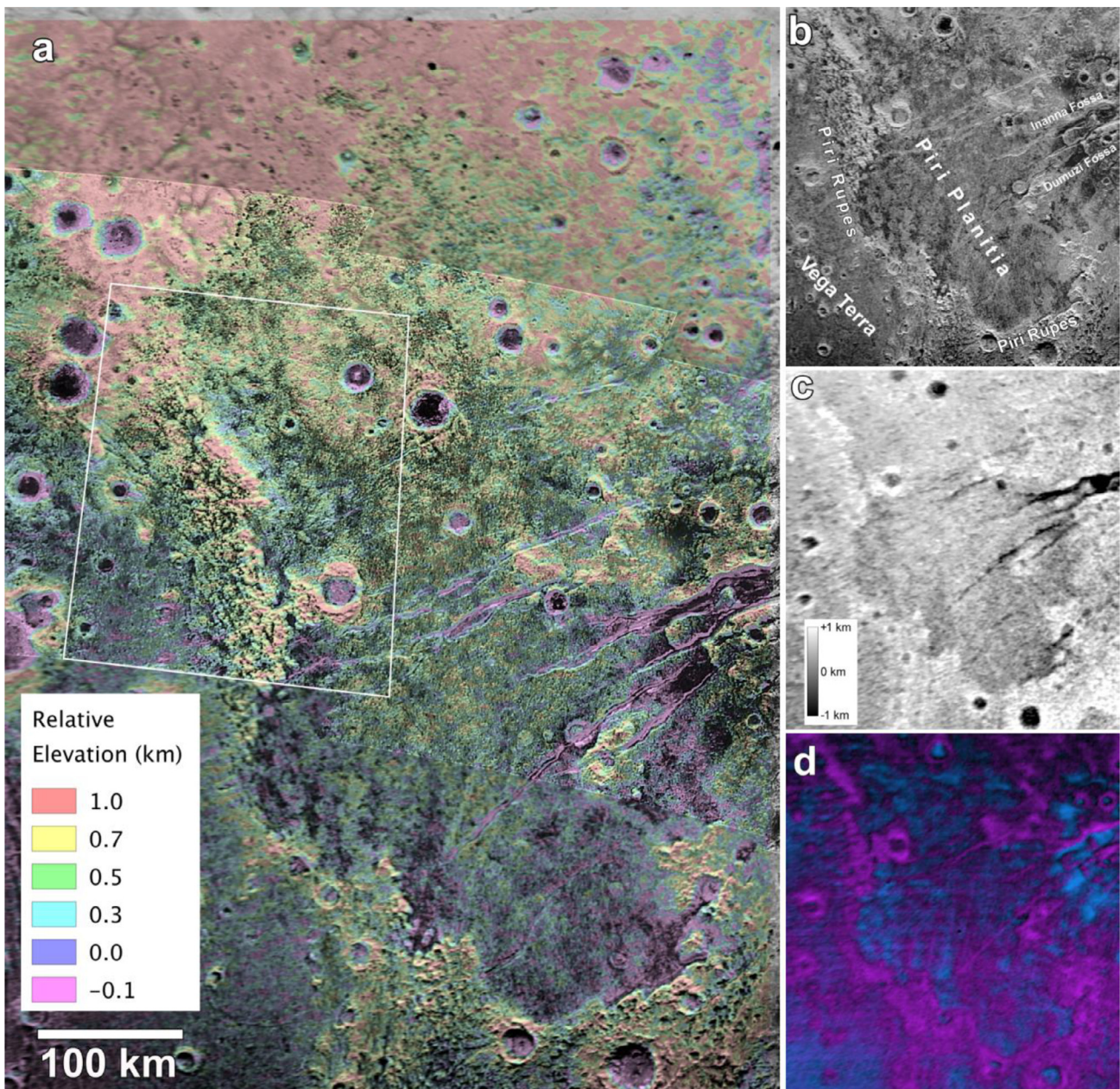
Fig. 7. Piri Planitia and Rupes. (a) A mosaic composed of the high resolution data sets of the region colorized with topographic data and centered at 30°N, 110°E, location of Fig. 8 outlined in white; (b) Informal names used for this region; (c) Digital Terrain Model of the Piri Planitia region where increasing brightness trends with increasing elevation; (d) Map of compositional information derived from the LEISA imaging spectrometer of the southern portion of Piri Planitia region. Purple indicates the presence of CH_4, and blue indicates the signature of H_2O. (Images used in mosaic (a) are 678 m/pixel P_CCOLOR_2 MVIC swath overlain by 232 m/pixel P_LEISA_HIRES LORRI images). North to top. Illumination from above.

of these consider the stress-strainrate behavior of methane ice grains of size d_g. For today's Pluto temperatures, and providing the basal stresses are relatively low, solid methane responds diffusively (Coble creep) and the relaxation rate is expressed in Eq. (A6) of Appendix. Adopting $d_g = 1\,mm, T = 40°K$ and mounds with slopes of about $\theta = 30°$, then the corresponding lifetime is about 42 Gyr (years are given in terrestrial years unless explicitly stated otherwise).

A recent laboratory study of annealed CH_4 ice (Yamashita et al., 2010) shows that solid methane responds with power law creep behavior. However, applying the results of this study indicates that structures, like that considered above (i.e., $H/L \approx 0.5 \leftrightarrow \theta \approx 30°$), would have lifetimes of about 3.2 months! This laboratory data was acquired for applied stresses well over 1 MPa and have been

applied here by extending its range of validity down by two orders of magnitude in stress. In a strict sense, therefore, we question whether these rheological data are relevant for these landforms.

An older study (Bolshutkin et al., 1968) also suggests that methane exhibits power-law creep ($n = 3$, with no noted grainsize dependence. n is experimentally determined, see Appendix) when stresses are relatively high (exceeding a few kPa). Calculations assuming this alternative rheology *for the whole of such structures* show that those with relatively steep grades, e.g., with $H/L \approx 0.5 \leftrightarrow \theta = 30°$, have short geological lifetimes of about 0.65 Myr. However, for the same value of H but with $H/L \approx 0.1 \leftrightarrow \theta \approx 7°$ then the corresponding lifetime is about 400 Myr. Of course, if structures like the pitted uplands are methane mounds, then their basal cores may be behaving as a material characterized by

Fig. 8. The highest resolution view of a portion of Piri Rupes, where it is seen along the west side of Piri Planitia (to the right), showing prominent pitting along its crests. Image is from reprojected 232 m/pixel LORRI coverage of the P_LEISA_HIRES observation, centered at 102.32°E, 33.18°N. Arrow points North. Illumination high and from above.

Fig. 10. Penitentes on a high altitude snowfield in Chile. Individual penitentes are typically 1 to 2 m high. Source: Cristian Ordenes (Flickr, CC BY 2.0) License: https://creativecommons.org/licences/by/2.0/legalcode.

power-law creep while the mound brims (being shallower as they surrounding the core) may be behaving according to Coble creep and, hence, may still be able to hold up the entirety of the structure. This scenario will be true provided the grain sizes are greater than 1 mm.

The disparity in conclusions derived from published research (outlined above) for the mechanical behavior of CH_4 ice under Pluto conditions leaves very open whether pure (even large grained) CH_4 ice is viable candidate for supporting hundreds of meters of topographic relief. This situation begs for future work both in the lab and in theory. However, if pure CH_4 ice turns out to be "weak" it still may play a role as the cohesive matrix binding together H_2O ice grains in an outcrop that is a mixture of both, analogous to how calcite cement binds together quartz sand grains in a sandstone. The loss of the CH_4 through sublimation disaggregates the scarp face causing retreat.

3.1. Landform evolution modeling

Because the pitted textures on Pluto are eroded into ices that have a high potential for sublimation at the range of surface temperatures, we have looked to analogous planetary landforms and models of their formation. Although the ablation hollows and penitentes on terrestrial ablating ice (e.g. Fig. 10) are much smaller in scale than the pitting on Pluto's ices (Fig. 2), we suggest that similar processes may be acting in both. In particular, we hypothesize that Pluto's pits develop because reflected solar radiation induces a pattern instability during sublimation erosion. We also suggest that the size of pits is controlled by the interaction of sublimation and ice creep.

Terrestrial suncups and penitentes have been the subject of considerable study and speculation. Early observers postulated a variety of processes that might play a role in pattern formation, including solar-induced melting or sublimation, wind, and albedo variations due to included or deposited dust (Matthes, 1934; Lliboutry, 1954; Amstutz, 1958). Penitentes form in conditions most analogous to Pluto, under direct solar illumination at high elevations with low atmospheric pressure and low humidity. Small penitentes have been created in laboratory settings by sublimation of cold ices by direct illumination (Bergeron et al., 2006). Natural penitentes can develop extreme roughness, with sharply-pointed divides and rounded troughs (Fig. 10). The dominance of ablation
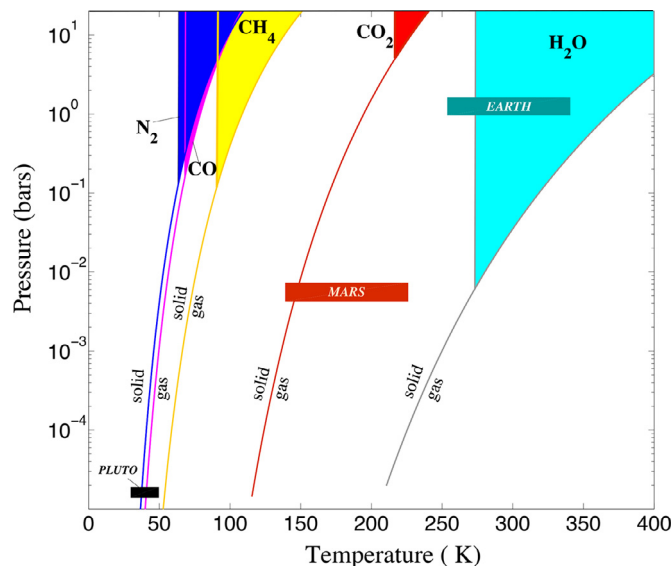
Fig. 9. Phase diagram for volatiles appearing on Pluto. Phase diagrams for N_2 (blue), CO (magenta) and CH_4 (yellow) are shown together with H_2O (aqua) and CO_2 (red) for comparison. Current day Pluto conditions indicated on bottom right while the conditions for Mars and the Earth are also indicated. Note that the liquid states of N_2 and CO overlap, as their respective triple points are close to one another. Evaporation/sublimation curves adapted from Fray & Schmitt (2009). Solid melt curves: N_2 from Scott (1976), CO from Goodwin (1985), CH_4 from Goodwin (1970). (For interpretation of the references to color in this figure legend, the reader is referred to the web version of this article.)

due to solar illumination is evidenced by the decay of penitentes under cloudy or windy conditions (Matthes, 1934; Amstutz, 1958).

We have implemented a heuristic exploratory model of pit development through sublimation erosion to explore conditions and mechanisms under which pits develop as well as the influence of simulation parameters on pit scaling and the sequence of relief development. The purpose of the modeling is to explore the main processes that may control the scale and spatial patterning of the sublimation pits in a simplified manner, and is not advanced as a comprehensive model of sublimation pit development. The model incorporates most of the assumptions in Betterton (2001), specifically (1) that pits develop through solar-induced sublimation whose rate is linearly proportional to intensity of illumination; (2) at any surface location the solar radiation includes both direct solar input plus light reflected from adjacent visible slopes; (3) that reflected light is diffuse and uniform in all directions (Lambertian); (4) that sublimation is a surface phenomenon such that the depth of light absorption and internal refraction is small compared to the scale of the resultant pits; (5) differential thermal heat transfer within the ice does not affect sublimation rates; and (6) surface albedo and ice properties are uniform and constant during sublimation (specifically that the ice does not include non-volatile components that accumulate on the surface or have a contrasting albedo). Sublimation rate is non-linearly related to illumination intensity, but the linear relationship is a first-order approximation. N_2 grain size variations with depth might affect albedo, but we have no way to constrain this. In addition thermal re-emission may contribute to sublimation, presumed to also obey assumptions (3) through (6).

An additional simplifying assumption is that sublimation occurs primarily during local noon. Penitentes have been observed on the Earth to have their axis of symmetry pointed toward the sun such that, for non-equatorial locations they are inclined (Lliboutry, 1954; Hastenrath and Koci, 1981; Post and LaCapelle, 2000). They do not form at high terrestrial latitudes both because of structural instability as well as less concentration of solar input near noon. In early stages of development penitentes tend to be elongated E-W, indicating a contribution of sublimation due to non-zenith sun angles (Amstutz, 1958). However, at advanced stages of penitente development shadowing becomes an important limit to the contribution of off-vertical illumination (Cathles et al., 2011; Cathles et al., 2014). Nevertheless, these same shadowed regions will continue to receive thermal re-radiation.

Sublimation erosion includes effects of both direct and reflected visible and thermal radiation. The direct radiation from a vertical sun produces a uniform vertical erosion independent of slope angle (unless overhanging) if sublimation rate is linearly proportional to illumination. If i is the incident light per unit horizontal area on the surface at noon, α is the surface albedo, K_s is the sublimation rate per unit absorbed light, and φ is the local slope gradient, then the rate of sublimation rate directed normal to the surface will be:

$$\frac{\partial n_d}{\partial t} = (1 - \alpha) i K_s \cos \varphi. \tag{1}$$

The vertical erosion rate, $\partial z_d / \partial t$, is inversely proportional to cos ϕ, so that:

$$\frac{\partial z_d}{\partial t} = \frac{\partial n_d}{\partial t} \cos^{-1} \varphi = (1 - \alpha) i K_s, \tag{2}$$

where the d subscript refers to sublimation due to direct illumination. In our model visualization, penitents will not form if vertical erosion overwhelms the driving effect of reflected light.

We do not model the direct illumination effect because it would be a constant additive term not, in itself, producing pitting. We do model sublimation resulting from reflected illumination and thermal scattering. We utilize a grid of cells of dimensions dx and dy
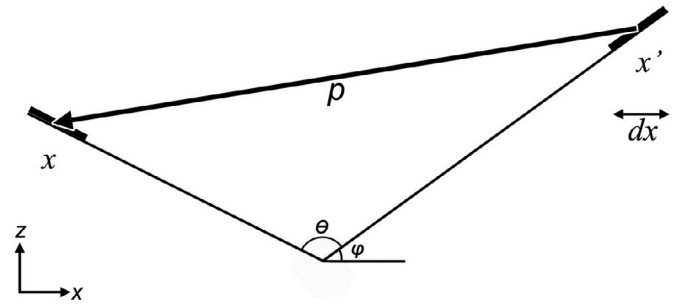
Fig. 11. Definition of relationships for reflected radiation from x' being received at x is proportional to the product of Cos θ/2 and $1/p2$ as used in the modeling described in the paper. See text for details.

with evolving vertical elevation (x, y, z). Fig. 11 shows, in cross section, the influx of reflected light dI, to the cell at location x from a cell at location x' at a separation distance, p, and the angle between their tangent lines, θ, which we approximate as

$$dI_r = i_r p^{-2} \cos(\theta/2) \, dx \, dy \tag{3}$$

where i_r is the intensity of the reflected light per unit surface area. At zenith i_r will depend upon the local slope gradient at the contributing site,

$$i_r = \alpha i \cos \varphi \tag{4}$$

where i is the solar illumination intensity, and φ is the slope angle at the contributing cell. The total reflected light input I_r is approximated by summing contributions from visible cells. The calculation of local sublimation rates using Eqs. (3) and (4) is accomplished by cycling through all cells in the matrix. At each cell the light reflected from neighboring cells is calculated by progressing outward from the target cell and evaluating reflected light contribution from each neighboring cell. For computational efficiency, only contributions from neighboring cells along cardinal and diagonal directions are used to calculate I_r for each target cell. This underestimates the total radiation input in direct proportion to the separation distance, x, so that the sum of calculated incident light for each separation distance is calculated using (1) and (2) and multiplied by x. For the simulations reported here, the maximum contributing distance, x, was 100 cells, but often smaller in depressions due to lack of visibility. This distance was much larger than the simulated pit sizes. The rate of erosion due to sublimation is calculated as

$$\frac{dz_r}{dt} = K_s I_r \alpha \cos^{-1} \phi, \tag{5}$$

where ϕ is the local slope angle and the subscript r refers to erosion by reflected light.

Surfaces eroded by sublimation according to Eq. (3)–(5) are inherently unstable because depressions always erode more rapidly than divides, and evolve into three simulation-cell width deep pits. The intricate pitted landscape shown in Fig. 10 approaches this infinite roughness. Several mechanisms may place a lower limit on pit dimensions, including thermal diffusion, atmospheric humidity gradients, and diffusive light transfer within the ice (Betterton, 2001; Mitchell, 2005; Tiedje et al., 2006; Mitchell and Tiedje, 2010). Tiedje et al. (2006) suggest that diffusive light transfer acts to diffuse sublimation and determine the minimum scale of terrestrial penitentes and sun cups. At the scale of Pluto's sublimation pits light diffusion is unlikely to be important, but the softness of nitrogen ice is likely to lead to creep diffusion that limits the depth and size of sublimation pits. We assume that the diffusive creep is shallow and limited by a maximum stable slope gradient, S_c. We adopt the widely-used non-linear creep model of (Roering et al., 1999, 2001) in which erosion of the surface due
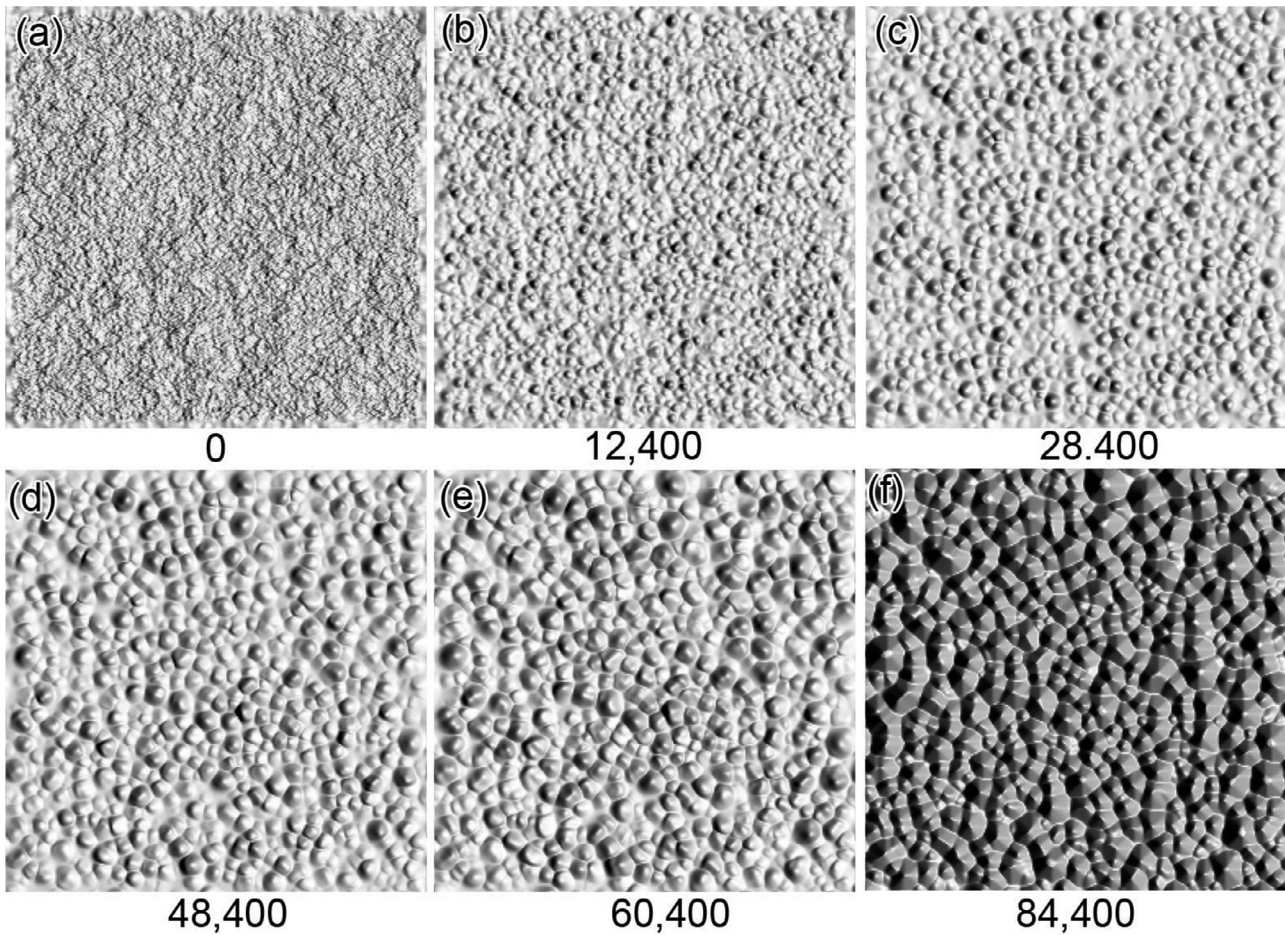
Fig. 12. Successive stages (iterations) of sublimation pit development through a combination of sublimation from reflected light and diffusive mass wasting. Numbers reflect to (arbitrary) relative time. See Fig. 13 for relief development during this simulation. Illumination is from the left in this and Figs. 13–15.

to ice creep is proportional to the spatial divergence of material flux:

$$\frac{dz_c}{dt} = -\nabla \cdot \left[\frac{K_c \nabla z}{1 - |\nabla z|^2 / S_c^2} \right], \qquad (6)$$

where ∇z is the vector slope gradient and S_c is a critical slope gradient which accounts for limitations on steepness or height of ice slopes. The overall erosion rate is the sum of $\partial z_d / \partial t$, dz_s/dt and dz_c/dt. In using Eq. (6) we equate creep of the surface N_2 ice to that of terrestrial regolith. For both cases the moving material is assumed to affect only a thin layer relative to the scale of the slope. Because sublimation erosion tends to increase roughness and creep to diffuse it, the horizontal scale of the resultant pitting is expected to increase as the ratio increases. $K_c/K_s I_r$ A detailed physics-based model of these phenomena, similar to what was done for Calisto (White et al., 2015), should and will be presented in a forthcoming study.

4. Example simulations

We implement the model on a doubly-periodic square 256×256 grid with 100 m square cells. We set $K_s I_r$ to unity and vary K_c to explore topographic evolution. The initial conditions are a pseudo-fractal surface of low fractal dimension and low relief, so that initial slopes are less than 0.01 (Fig. 12a). A random surface was selected to illustrate scale selection by the model and the intrinsic instability of a nearly flat surface. During the initial stages relief development is concentrated within the most prominent depressions in the initial fractal surface (Fig. 12b and c). Di-

vides exhibit minimal erosion as pits deepen. As pits continue to deepen and widen, their edges begin to intersect (Fig. 12d and e). During the final stages of the simulation the pit walls intersect at sharp divides, creating a cellular pattern with pit walls approaching the critical slope steepness, S_c (Fig. 12e and f). As pits enlarge, some pits merge, increasing the average size of the pits by a factor of about two between the timelines (b) and (f) in Fig. 12. The Sputnik Planitia pits shown in Fig. 4a and b have a pattern similar to Fig. 12e and f, suggesting pits have enlarged to the stage of shared divides. It is uncertain, however, whether sideslope gradients of the Sputnik Plantia pits reach the ~32° gradient typical of threshold slope mass wasting. Stereo imaging reveals, however, that the large, deep pits on the Pitted Uplands have sideslopes commensurate with threshold mass wasting (Figs. 2–4).

Relief development is strongly non-linear in time, with a long period of slow relief increase followed by explosive growth as illumination focusing becomes more prevalent (Fig. 13). Because the simulations only model erosion due to reflected light, divides do not appreciably erode until pit walls merge and diffusive mass wasting becomes important. If sublimation due to direct illumination were included in the model, there would be steady, spatially uniform erosion superimposed on the topographic evolution shown in Fig. 13. A similar pattern of slow initial growth followed by rapid erosion to form a cellular network of pits was observed in suncup modeling by Tiedge et al. (2006) using the sum of a negative Laplacian, $-c_1 \nabla^2 z$, which roughens the surface, and $-c_2 \nabla^4 z$, which tends to smooth the surface. The ratio of c_2/c_1 determines the scale of the pits.
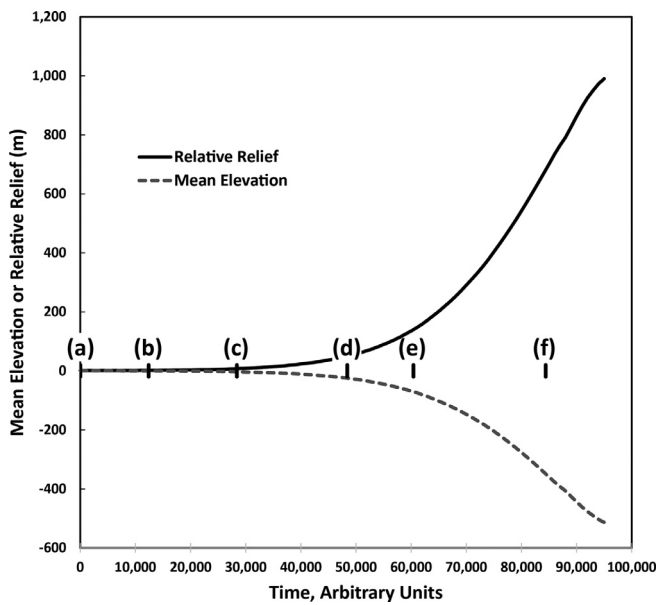
Fig. 13. Development of relief during simulation pit development in Fig. 12. Letters correspond to illustrated iterations in Fig. 12.

The effect of varying the ratio of mass wasting diffusivity to sublimation rate is shown in Fig. 14, where the simulation in Fig. 14 (right) has a diffusivity, K_c, 10 times that in Fig. 14 (left). In this case sublimation is only competing with mass wasting for large pits. Sublimation scaling, $K_s I_r$, was the same for both simulations as was the total simulated time. By itself, sublimation would tend to form infinitely small pits (e.g., penitentes), but mass wasting destroys small pits in proportion to its intensity (higher diffusivity). Because the change in pit scale during pit development for constant parameter values is small, the large spatial variability in pit scales in Fig. 2 is likely due to variation in substrate properties affecting the ratio $K_c/(K_s I_r)$, or possibly to a more complicated spatial-temporal evolution of the pits.

Pits on Sputnik Planitia and the Pitted Uplands commonly show preferential elongation, either as isolated elongated pits (the "bacilli", Figs. 3 and 4d or as pit chains (Figs. 2, 4b and e). We have explored preferential directional pit development by increasing sublimation rates for slopes facing NE by a factor of three relative to slopes facing in other directions. This produces elongated pits and pit chains similar to the preferential alignments on Sputnik Planitia noted above (Fig. 15), although we have discussed above other processes that could cause elongated pits.

We also conducted simulations eliminating the denominator term in Eq. (6) such that ice diffusion is linear in slope gradient. The spatial pattern of pit development is similar to the simulations using non-linear creep and the spatial scale of the resultant pits of the resultant pits is likewise proportional to the creep diffusivity, K_c. The relief and interior pit wall gradients, however, increase to very high values during such simulations, producing morphologies similar to the peninentes in Fig. 10. Future analysis of pit morphology using photoclinometry will estimate depths and wall steepnesses of sublimation pits on Sputnik Planitia, which should provide the basis for more accurate modeling of the role of diffusion in limiting pit size and steepness.

Our simple model does not replicate the entire spectrum of pit morphologies shown on Sputnik Planitia or the Pitted Uplands. For example, the isolated pits shown in Fig. 4f or the isolated "bacilli" (Figs. 3 and 4d) are not produced by the model. It may be that there is a threshold for pit development, perhaps related to a layered ice structure, or related to non-linear sublimation pro-

cesses, such as specular reflection. Temporal variations in processes may also be a factor. For example, subtle "dimples" in the terrain of Fig. 4f could be pits which have become inactive and are being destroyed by diffusive mass wasting. Why this should occur is uncertain. Possibilities include surface accumulation of less-volatile ices and ice temperature increase enhancing lateral creep, among others. The model assumes that the diffusion occurs over a depth scale much less than the spatial pit scale. This might be appropriate if diffusion occurs primarily through thermal diffusion from seasonal solar illumination. If, however, diffusion occurs over depths commensurate with pit scales, the topographic evolution will more resemble relaxation of impact craters in ice, possibly involving bulbous uplift of the pit centers (Thomas and Schubert, 1987; Thomas and Schubert, 1988; Thomas and Squyres, 1988; and see below).

The observed systematic patterns of pit density and depth associated with the large convective cells such that convective cell centers often have low-relief pitting and cell edges have smooth surfaces or sparse, shallow pitting (Fig. 5) could be due to several process interactions, including: (1) systematic surface age variation; (2) thermal effects due to convective cell motion; or (3) compositional effects. The centers of cells are interpreted to be locations of upwelling and the cell edges as sites of downwelling, with a surface ice flow from the center to the edges (McKinnon et al., 2016; Umurhan et al., this issue). The surface age explanation for the annular pattern of deep pitting may be related to the long gestation of sublimation pit development followed by explosive growth (Fig. 13) coupled with increasing surface age from cell center to edge. A high heat gradient near the central upwellings might decrease the mean viscosity of the near-surface ice, healing incipient pits through diffusive flow. Compositional effects might play a role in that ice composition may vary with surface age due to sublimation stripping of the surface, altering the ice mixture (either in the admixture of ices or in grain size). None of these explanations readily account for the sparse, shallow pitting along cell boundaries/vertices, which suggests possible decay of former deeper and denser pitting.

In conclusion, our heuristic model shows how pit formation due to insolation can interact with ice creep to determine the horizontal and vertical scales of sublimation pitting on Pluto. Hopefully, future modeling with less-restrictive assumptions (e.g., Hecht, 2002; Cathes et al., 2014; Claudin et al., 2015) can explore the details of sublimation pit development on Pluto.

5. Timescales

The results shown in Fig 14 suggest that the pits evolve until the timescales of sublimation and mass wasting are comparable. Although there are very large uncertainties, it is clearly of interest to explore what absolute timescales are implied. Except for the non-linear component, mass wasting (Eq. (4)) is a diffusive process, and so too is viscous relaxation. If the mass wasting is a consequence of viscous flow, the characteristic timescale of either process may be written as (Melosh 1989)

$$t_R \sim \frac{2\eta k}{\rho g} f(kd) \tag{7}$$

where η is the (Newtonian) viscosity, k is the wavenumber ($\sim \pi/D$, where D is the diameter of the feature), ρ is density, g is surface gravity, d is the thickness of the flowing layer, and f is a function which depends on the product kd. For mass wasting, the flowing layer is thin compared to D, so that $kd \ll 1$ and, in this limit, the leading order dependence on $f(kd) \sim (kd)^{-3}$ (Melosh 1989). For viscous relaxation, if the layer thickness is larger than D ($kd > 1$), we have $f(kd) \sim 1$. As expected, flow in a thin, creeping layer results in much longer modification timescales than viscous
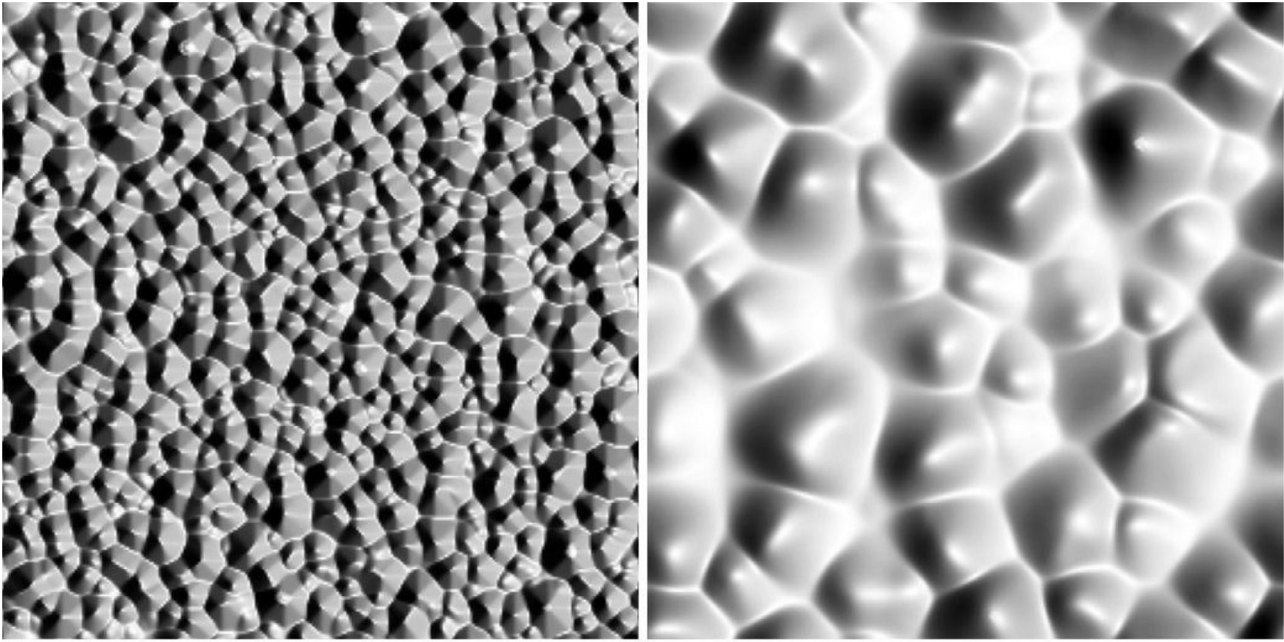
Fig. 14. Difference in scale of pitting as ratio of mass wasting rate to sublimation rate is varied over a factor of 10. Both simulations were conducted for the same total simulated time and identical sublimation scaling, Kslr. The coarse pitting (right) has the same intensity of sublimation but 10 times the slope diffusivity, so that sublimation can only compete with mass wasting for large pits. By itself, sublimation would tend to form infinitely small pits (e.g., penitentes), but mass wasting destroys small pits in proportion to its intensity (higher diffusivity).
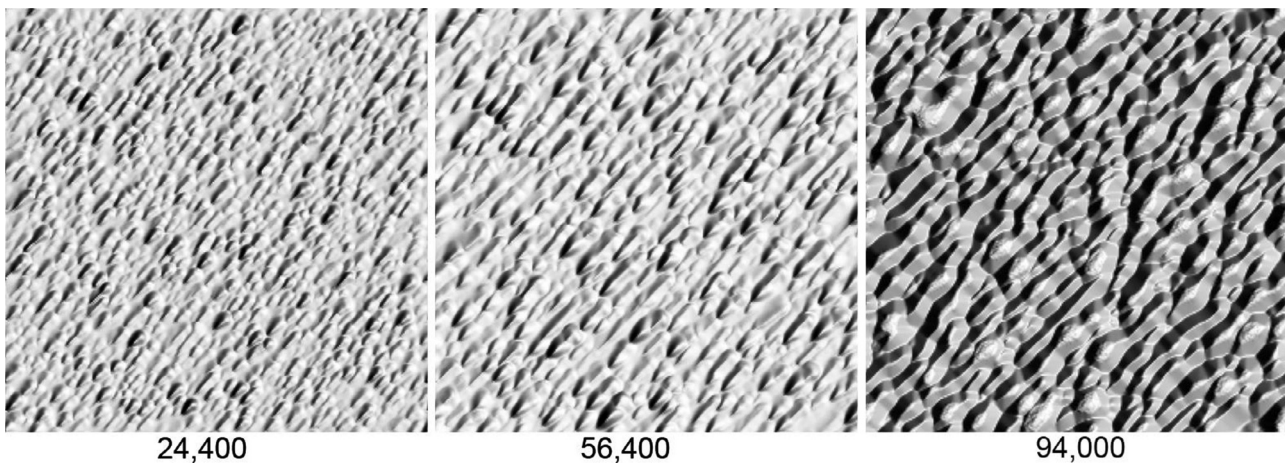
Fig. 15. Development of sublimation pits in which slopes facing to upper left sublimate 3 times more rapidly than comparable slopes facing in other directions. Numbers are simulation model times.

relaxation. The N_2 ice layer in Sputnik Planitia is probably several km thick (McKinnon et al. 2016) so one might expect that $kd > 1$. The only available measurements of N_2 ice rheology were performed by Yamashita et al. (2010). These authors find that at stresses of order 0.1 MPa the effective viscosity of N_2 ice at Pluto's surface is about 10^{10} Pa s. The presence of secondary phases (such as CH_4) and/or grain-size sensitive effects could increase this viscosity significantly. Nonetheless, taken at face value the implied viscous relaxation timescale for a 1 km diameter pit would then be about a terrestrial day, indicating that Yamashita et al. (2010) results are inconsistent with the observation of pits on SP. The divergence in the values given for rheological properties of N2 (e.g., Eleuskiwicz and Stevenson, 1990; Yamashita et al., 2010) demonstrate that N2 ice rheology is currently poorly constrained. However, the 1 Myr convective overturn timescale derived in McKinnon et al. (2006) serves as an upper limit to the timescale on which viscous relaxation could destroy/erase pits.

6. Conclusions

Fields of pits, both large and small, in Tombaugh Regio (Sputnik Planitia and the Pitted Uplands to the east), and along the scarp of Piri Rupes, are examples of landscapes on Pluto where we conclude that sublimation drives their formation and evolution. Our heuristic modeling closely mimics the form, spacing, and arrangement of a variety of Tombaugh Regio's pits. Our modeling suggests that Pluto's sublimation modified landforms appear to require an additional significant role for (diffusive) mass wasting in a thin layer. In our models, the temporal evolution of pitted surfaces is such that considerable time passes with little happening, then eventually, very rapid development of relief and rapid sublimation. The small size and depth of the pits on Sputnik Planitia are consistent with them being formed in N_2-ice, which is also the most volatile of the major ices on Pluto's surface with some component of CO ice, which has similar physical properties. As N_2-ice

readily flows, some other "stiffer" volatile ice may play a role in supporting the relief of sublimation degraded landforms, such as scarps of Piri Planitia and the septa of the pitted uplands of east Tombaugh Regio, which exhibit relief of a few hundred meters. A strong candidate is CH_4, which is observed at these locations. Our current state of knowledge regarding the rheological properties of CH_4 on Pluto's surface is unfortunately ambiguous. We strongly encourage new research toward the determination of the mechanical properties of CH_4 at Pluto conditions. As was discussed in Moore et al. (2016), we strongly suspect that sublimation erosion also has played a significant role in the development of the Bladed terrain of Tartarus Dorsa (centered roughly 20°N, 225°E) and the large deep pits of the Arctic Eroded Mantle terrain (centered roughly 60°N, 210°E), but we also think that their histories are complex, involving several other processes, and thus they are the subjects of separate ongoing studies.

Acknowledgements

Appendix

The rheology of CH_4 under the surface pressures and temperatures appropriate for modern day Pluto is based on two groupings of studies found in the literature. For the sake of completeness, we review them here and offer some quantitative numbers for consideration with regards to the ability of CH_4 to uphold topography of various dimensions and scales. In the discussion that follows we present a mathematically pedagogical discussion.

Eluszkiewicz and Stevenson (1990, ES90 hereafter) and Eluszkiewicz (1991, E91 hereafter) examine the elastic creep properties of CH_4 grains based on nuclear magnetic resonance experiments performed in the late 1970's. The stress-strain relationship in such materials can be written as a sum of two processes, namely, volume diffusion (Nabarro–Herring creep, NH hereafter) and boundary diffusion (Coble creep):

$$\dot{\epsilon} = \dot{\epsilon}_v + \dot{\epsilon}_b, \tag{A1}$$

in which $\dot{\epsilon}$ is the strain rate and $\dot{\epsilon}_v$, $\dot{\epsilon}_b$ are the aforementioned creep mechanisms. The NH creep (volume diffusion) rate, which is generally active when the material is close to its melt temperature, is given by

$$\dot{\epsilon}_v = \frac{42 D_{0v} \Omega \sigma}{kT d_g^2} e^{-E_v/kT}, \tag{A2}$$

where k is the Boltzmann constant, T is temperature, d_g is grain size, Ω is the volume of a single molecule of CH_4, $5.11 \times 10^{-29} m^3$, σ is the applied stress, the experimentally measured value of the molecular diffusion rate is $D_{0v} = 10^{-3}$ m²/s, while the activation energy for volume diffusion in CH_4 crystals was measured to be $E_v = 15.9$ kJ/mole. We often refer to the corresponding "activation temperature" instead of the activation energy, where in this case of volume diffusion it is defined as $T_v = E_v/R = 1913 \, K$, where R is the universal gas constant (8.31 J/mole).

The corresponding formulation for Coble creep is given by

$$\dot{\epsilon}_b = \frac{42(2\pi\delta) D_{0b} \Omega \sigma}{kT d_g^3} e^{-E_b/kT}, \tag{A3}$$

where δ is the thickness of the boundary diffusion layer between grains, assumed to be the diameter of a single molecule of CH_4.

For our estimate purposes, here we assume that $\delta = \Omega^{1/3}$. To the knowledge of these authors, there is no published laboratory data on the boundary diffusion coefficient nor on the activation energies of Coble creep in CH_4 ice grains. In lieu of this data and following both ES90 and E91, we assume that $D_{0b} \approx D_{0v}$. Similarly following ES90 who, in turn, followed the suggestion of Ashby and Verall (1978), we assume that $E_b = (2/3)E_v$, which translates to a corresponding Coble creep activation temperature of $T_b = 1311$ K.

It is worthwhile to assess for what combinations of temperature and grain size NH creep dominates Coble creep. We define the critical temperature T_c at which NH creep and Coble creep are of equal magnitude, i.e., when $\dot{\epsilon}_b = \dot{\epsilon}_v$. After inserting into this equation the corresponding expressions for the two creep mechanisms, followed by sorting through the algebra, results in the simple expression

$$T_c = \frac{T_b}{2 \ln\left(d_g/2\pi\,\Omega^{1/3}\right)}, \tag{A4}$$

where, if we assume 1 mm grains, we find $T_c \approx 50.5$ K. According to this relationship, taking the present-day surface temperature of Pluto to be around 40 K, Coble creep in CH_4 ice grains is dominant. In fact, the ratio of the creep rates maybe expressed by the following formula

$$\frac{\dot{\epsilon}_b}{\dot{\epsilon}_v} = \left(\frac{1\,mm}{d_g}\right) \exp\left(\frac{T_v}{3T} - \frac{T_v}{3T_c}\right); \tag{A5}$$

and for 1 mm ice grains we find $\dot{\epsilon}_b/\dot{\epsilon}_v \approx 27.5$. Focusing therefore on Coble creep, we may rewrite its stress-strainrate expression in terms of quantities more readily amenable to our following considerations, that is to say,

$$\dot{\epsilon}_b = 1.49 \times 10^{-15} \text{ Pa}^{-1} \text{ yr}^{-1} \sigma \left(\frac{1\,mm}{d_g^3}\right)\left(\frac{40\,K}{T}\right)$$
$$\times \exp\left(\frac{1311}{40} - \frac{1311\,K}{T}\right). \tag{A6}$$

Because this creep mechanism is linear with respect to the applied stress (aka: diffusional creep), we may immediately estimate the e-folding relaxation time for structures of interest: Suppose we have a pure methane structure ("mound") of height H and horizontal scale $2L$, and we further suppose the base of the structure sits on an infinitely strong bedrock structure. The tangential stresses at the base of the structure may be approximated by $\sigma = \rho g H \sin\theta$ where θ is the typical sloping angle of the structure with respect to the horizontal, which may be estimated by $\sin\theta \approx \theta = H/L$ for values of $H/L < 0.2$. Following typical arguments of creeping solid-state flow (e.g. Benn & Evans, 2010), the rate of change in the local mass content of a massive column is proportional to the height of the column, H, divided by a relaxation time τ. Meanwhile, the mass-flux rate through this column is $q \sim H^2 \dot{\epsilon}$, thus the rate of adjustment of a column of height H is equated to the local divergence of the mass-flux $\nabla \cdot q$, the latter of which we estimate with $\approx q/L$. Thus, equating these two, i.e. H/τ and q/L, gives an estimate for the e-folding inverse relaxation time for CH_4 structures *subject to Coble creep*, and is given by the following expression:

$$\frac{1}{\tau} \approx \frac{H}{L}\dot{\epsilon}_b \approx 1.49 \times 10^{-15} \left(\frac{H}{L}\right)^2 \left(\frac{\rho g H}{\text{Pa}}\right)\left(\frac{1mm}{d_g^3}\right)\left(\frac{40\,K}{T}\right)$$
$$\times \exp\left(\frac{1311}{40} - \frac{1311\,K}{T}\right) \text{yr}^{-1}. \tag{A7}$$

Mounds with heights of about 300 m together with horizontal scales of about 3 km have $\theta \approx H/L \sim 0.1$, while the pressure at their bases are given by $\rho g H = 8.37 \times 10^4$ Pa, or nearly 1 bar – which means the corresponding tangential stresses at their bases are on the order of 0.1 bar (0.01 MPa). At 40 K a structure composed primarily of 1 mm CH_4 ice grains will have an e-folding lifetime $\tau \approx 700$ Byr. For 0.2 mm ice grains, τ is about 5.6 Byr.

As noted by ES90, the transition from diffusional flow to plastic flow (in which the strainrate dependence on applied stress is nonlinear) in CH_4 ices might occur when stresses exceed 0.01 bars. This supposition was based on creep parameter measurements made by Bolshutkin et al. (1968). However, the dependence of the creep parameters on neither grainsize nor for strain-rates appropriate for geologic timescale processes (especially relevant for the conditions in the outer solar system) were determined. Extrapolation of their results, which were assessed for strain-rates $>10^{-7}$ s^{-1}, to circumstances appropriate to Pluto would involve stretching their results across many orders of magnitude. Nonetheless, ES91 suggest that based on the experiments of Bolushkin et al. (1968), the power-law (plastic) creep parameters obey $\dot{\epsilon}_p = A\sigma^n \exp(-T_p/T)$, where the power-law creep activation temperature is $T_p = E_p/R \approx 1000$ K, in which E_p was experimentally determined as well. The other remaining parameters were also experimentally determined, $n \approx 3$ and $A \approx 10$ MPa^{-n} s^{-1}. Applying the same argument as before, and inserting the above assumed numbers appropriate for the pitted uplands and Piri Rupes with T = 40 K, the e-folding relaxation timescale in this power-law creep regime would follow $\tau^{-1} \sim (H/L)\dot{\epsilon}_p \approx 2.6 \times 10^{-9}$ yr^{-1}, or approximately 400 Myr.

A more recent experimental study of *laboratory annealed* CH_4, reported by Yamashita et al. (2010), shows that the plastic flow strain-rate of methane responds on much shorter timescales. In this particular result, Yamashita et al. (2010) demonstrate that the stress-strainrate relationship of annealed CH_4 behaves according to

$$\dot{\epsilon}_a = A\sigma^n \tag{A8}$$

where at 45 K $A = 10^{-4}$ MPa^{-n} s^{-1}, with $n \approx 1.9$. Then following the argument given before, the relaxation timescale under these circumstances would follow

$$\frac{1}{\tau} \approx \frac{H}{L}\dot{\epsilon}_a = A\left(\frac{H}{L}\right)^{n+1}(\rho g H)^n, \tag{A9}$$

and, applying the dimensions we have considered above for the model terrain we consider would result in a relaxation time of $\tau^{-1} = 0.39$ yr^{-1}, or about 2.5 years which is an answer that is 9 orders of magnitude different than the corresponding analysis done in the diffusion limit! We note here that the study done in Yamashita et al. (2010) did not consider stresses below 1 MPa, which are two orders of magnitude larger than the estimated stresses at the base of the pitted uplands and Piri Rupes. The main differences, however, seem likely to be in the differences between annealed CH_4 ice versus CH_4 ice grains.

Further laboratory studies are needed to both resolve these discrepancies between the two power-law creep studies and, moreover, to reproduce the general ice-grain results discussed in the beginning of this section.

References

Amstutz, G.C., 1958. On the formation of snow penitentes. J. Glaciol. 3 (304-311).

Ashby, M.F., Verall, R.A., 1978. Micromechanisms of flow and fracture, and their relevance to the rheology of the upper mantle. Phil. Trans. R. Soc. Lond. 288, 59–95.

Barnhart, C.J., Howard, A.D., Moore, J.M., 2009. Long-term precipitation and late-stage valley network formation: landform simulations of parana Basin, mars. J. Geophys. Res. 114, E01003. doi:10.01029/02008JE003122.

Benn, D.I., Evans, D.J.A., 2010. Glaciers and Glaciation, 2nd edition Routledge, NY.

Bergeron, V., Berger, C., Betterton, M., 2006. Controlled irradiative formation of penitentes. Phys. Rev. Lett. 96 (9).

Betterton, M., 2001. Theory of structure formation in snowfields motivated by penitentes, suncups, and dirt cones. Phys. Rev. E 63 (5).

Bolshutkin, D.N., Borisova, L.I., Leonteva, A.V., 1968. Creep of crystalline methane. Sov. Phys. Solid State 10, 1248–1249.

Byrne, S., Ingersoll, A.P., 2003. A sublimation model for martian south polar ice features. Science 299 (5609), 1051–1053.

Cathles, L.M., Abbot, D.S., Bassis, J.N., MacAyeal, D.R., 2011. Modeling of surface-roughness/solar-ablation feedback: application to small-scale surface channels and crevasses of the Greenland ice sheet. Ann. Glaciol. 52 (59), 99–108. doi:10.3189/172756411799096268.

Cathles, L.M., Abbot, D.S., MacAyeal, D.R., 2014. Intra-surface radioactive transfer limits the geographic extent of snow penitents on horizontal snowfields. J. Glaciol. 60 (219), 147–154. doi:10.3189/2014JoG3113J3124.

Cheng, A.F., Weaver, H.A., Conard, S.J., Morgan, M.F., Barnouin-Jha, O., Boldt, J.D., Cooper, K.A., Darlington, E.H., Grey, M.P., Hayes, J.R., 2008. Long-range reconnaissance imager on new horizons. Space Sci. Rev. 140, 189–215. http://dx.doi.org/10.1007/s11214-007-9271-6.

Chyba, C., Sagan, C., 1990. Triton's streaks as windblown dust. Nature 346, 546–548.

Claudin, P., Jarry, H., Vignoles, G., Plapp, M., Andreottin, B., 2015. Physical processes causing the formation of penitentes. Phys. Rev. E 92, 033015. doi:10.1103/PhysRevE.92.033015.

Dundas, C.M., Byrne, S., McEwen, A.S., 2015. Modeling the development of martian sublimation thermokarst landforms. Icarus 262, 154–169.

Eluszkiewicz, J., 1991. On the microphysical state of the surface of triton. J. Geophys. Res 96.

Eluszkiewicz, J., Stevenson, D.J., 1990. Rheology of solid methane and nitrogen - applications to triton. Geophys. Res. Lett. 17, 1753–1756.

Forsberg-Taylor, N.K., Howard, A.D., Craddock, R.A., 2004. Crater degradation in the martian highlands: morphometric analysis in the sinus sabaeus region and simulation modeling suggest fluvial processes. J. Geophys. Res. 109. doi:10.1029/2004JE002242.

Fray, N., Schmitt, B., 2009. Sublimation of ices of astrophysical interest, a bibliographic review. Planet. Space Sci. 57, 2053–2080.

Goodwin, R.D., 1970. Thermophysical properties of methane: virial coefficients, vapor and melting pressures. J. Res. Nation. Bureau Stand., A. 74A (5), 655–660.

Goodwin, R.D., 1985. Carbon monoxide properties from 68 to 1000 K at pressures to 100 Mpa",. J. Phys. Chem. Ref. Data 14 (4), 849–932.

Grundy, W.M., Binzel, R.P., Buratti, B.J., Cook, J.C., Cruikshank, D.P., Dalle Ore, C.M., Earle, A.M., Ennico, K., Howett, C.J.A., Lunsford, A.W., Olkin, C.B., Parker, A.H., Philippe, S., Protopapa, S., Reuter, D.C., Schmitt, B., Singer, K.N., Verbiscer, A.J., Beyer, R.A., Buie, M.W., Cheng, A.F., Jennings, D.E., Linscott, I.R., Parker, J.W., Schenk, P.M., Spencer, J.R., Stansberry, J.A., Stern, L.A., Throop, H.B., Tsang, C.C.C., Weaver, H.A., Young, L.A., 2016. Surface compositions across Pluto and charon. Science, in press.

Hastenrath, S., Koci, B., 1981. Micro-morphology of the snow surface at the quelccaya ice cap. Peru. J. Glaciol. 27 (97), 423–428.

Hecht, M.H., 2002. Metastability of liquid water on mars. Icarus 156, 373–386. doi:10.1006/icar.2001.6794.

Howard, A.D., 1978. Origin of the stepped topography of the martian poles. Icarus 34, 581–599.

Howard, A.D., 1994. A detachment-limited model of drainage-basin evolution. Water Resour. Res. 30 (7), 2261–2285.

Howard, A.D., 2000. The role of eolian processes in forming surface features of the martian polar layered deposits. Icarus 144, 267–288.

Howard, A.D., 2007. Simulating the development of martian highland landscapes through the interaction of impact cratering, fluvial erosion, and variable hydrologic forcing. Geomorphology 91, 332–363.

Howard, A.D., Breton, S., Moore, J.M., 2016. Formation of gravel pavements during fluvial erosion as an explanation for persistence of ancient cratered terrain on titan and mars. Icarus 270, 100–113. http://dx.doi.org/110.1016/j.icarus.2015.1005.1034.

Howard, A.D., Moore, J.M., 2008. Sublimation-driven erosion on Callisto: a landform simulation model test. Geophys. Res. Lett. 35, L03203. doi:10.01029/02007GL032618.

Howard, A.D., Moore, J.M., Schenk, P.M., White, O.L., Spencer, J.R., 2012. Sublimation-driven erosion on Hyperion: topographic analysis and landform simulation model tests. Icarus 220, 268–276.

Kieffer, H.H., 2007. Cold jets in the martian polar caps. J. Geophys. Res. 112, E08005. doi:10.01029/02006JE002816.

Lange, A.L., 1959. Introductory notes on the changing geometry of cave structures. Cave Stud. 11.

Lliboutry, L., 1954. The origin of penitents. J. Glaciol. 2, 331–338.

Mangold, N., 2011. Ice sublimation as a geomorphic process: a planetary perspective. Geomorphology 126 (1-2), 1–17.

Matthes, F.E., 1934. Ablation of snow-fields at high altitudes by radiant solar heat. Trans. Am. Geophys. Union 15 (2), 380–385.

McKinnon, W.B., et al., 2016. Convection in a massive volatile ice layer maintains Pluto's geological and atmospheric vigour. Nature 534, 82–85. doi:10.1038/nature18289.

Melosh, H.J., 1989. Impact Cratering: A Geologic Process. Oxford Univ. Press, p. 245.

Mitchell, K.A., 2005. Chaotic Pattern Dynamics on Sun-Melted Snow. M.S., University of British Columbia, Vancouver, p. 89.

Mitchell, K.A., Tiedje, T., 2010. Growth and fluctuations of suncups on alpine snowpacks. J. Geophys. Res. 115 (F4). doi:10.01029/02010JF001724.

Moore, J.M., et al., 1999. Mass movement and landform degradation on the icy Galilean satellites: results of the Galileo nominal mission. Icarus 140, 294–312.

Moore, J.M., Howard, A.D., Schenk, P.M., McKinnon, W.B., Pappalardo, R.T., Ewing, R.C., Bierhaus, E.B., Bray, V.J., Spencer, J.R., Binzel, R.P., Buratti, B., Grundy, W.M., Olkin, C.B., Reitsema, H.J., Reuter, D.C., Stern, S.A., Weaver, H., Young, L.A., Beyer, R.A., 2015. Geology before Pluto: pre-encounter considerations. Icarus 246, 65–81. doi:10.1016/j.icarus.2014.1004.1028.

Moore, J.M., McKinnon, W.B., Spencer, J.R., Howard, A.D., Schenk, P.M., Beyer, R.A., Nimmo, F., Singer, K.N., Umurhan, O.M., White, O.L., Stern, S.A., Ennico, K., Olkin, C.B., Weaver, H.A., Young, L.A., Binzel, R.P., Buie, M.W., Buratti, B.J., Cheng, A.F., Cruikshank, D.P., Grundy, W.M., Linscott, I.R., Reitsema, H.J., Reuter, D.C., Showalter, M.R., Bray, V.J., Chavez, C.L., Howett, C.J.A., Lauer, T.R., Lisse, C.M., Parker, A.H., Porter, S.B., Robbins, S.J., Runyon, K., Stryk, T., Throop, H.B., Tsang, C.C.C., Verbiscer, A.J., Zangari, A., Chaikin, A.L., Wilhelms, D.E., Team, NewHorizonsScience, 2016. The geology of Pluto and charon through the eyes of new horizons. Science 351 (6279), 1284–1293.

Moore, J.M., Mellon, M.T., Zent, A.P., 1996. Mass wasting and ground collapse in terrains of volatile-rich deposits as a solar system-wide geological process: the pre-Galileo view. Icarus 122, 63–78.

Piqueux, S., Christensen, P.R., 2008. North and south subice gas flow and venting of the seasonal caps of Mars: a major geomorphological agent. J. Geophys. Res. 113 (E6).

Post, A., LaCapelle, E.R., 2000. Glacier Ice. University of Washington Press, Seattle.

Reuter, D.C., et al., 2008. Ralph: a visible/infrared imager for the new horizons Pluto/kuiper belt mission. Space Sci. Rev. 140, 129–154. http://dx.doi.org/10.1007/s11214-008-9375-7.

Rhodes, J.J., Amstrong, R.L., Warren, S.G., 1987. Mode of foration of "ablation hollows" controlled by dirt content of snow. J. Glaciol. 33 (114), 135–139.

Roering, J.J., Kirchner, J.W., Dietrich, W.E., 1999. Evidence for nonlinear, diffusive sediment transport on hill slopes and implications for landscape morphology. Water Resour. Res. 35 (3), 853–870.

Roering, J.J., Kirchner, J.W., Sklar, L.S., Dietrich, W.E., 2001. Hillslope evolution by nonlinear creep and landsliding: an experimental study. Geology 29 (2), 143–146.

Scott, T.A., 1976. Solid and liquid nitrogen. Phys. Rep. 27 (32), 89–157.

Stern, S.A., Bagenal, F., Ennico, K., Gladstone, G.R., Grundy, W.M., McKinnon, W.B., Moore, J.M., Olkin, C.B., Spencer, J.R., Weaver, H.A., Young, L.A., Andert, T., Andrews, J., Banks, M., Bauer, B., Bauman, J., Barnouin, O.S., Bedini, P., Beisser, K., Beyer, R.A., Bhaskaran, S., Binzel, R.P., Birath, E., Bird, M., Bogan, D.J., Bowman, A., Bray, V.J., Brozovic, M., Bryan, C., Buckley, M.R., Buie, M.W., Buratti, B.J., Bushman, S.S., Calloway, A., Carcich, B., Cheng, A.F., Conard, S., Conrad, C.A., Cook, J.C., Cruikshank, D.P., Custodio, O.S., Dalle Ore, C.M., Deboy, C., Dischner, Z.J.B., Dumont, P., Earle, A.M., Elliott, H.A., Ercol, J., Ernst, C.M., Finley, T., Flanigan, S.H., Fountain, G., Freeze, M.J., Greathouse, T., Green, J.L., Guo, Y., Hahn, M., Hamilton, D.P., Hamilton, S.A., Hanley, J., Harch, A., Hart, H.M., Hersman, C.B., Hill, A., Hill, M.E., Hinson, D.P., Holdridge, M.E., Horanyi, M., Howard, A.D., Howett, C.J.A., Jackman, C., Jacobson, R.A., Jennings, D.E., Kammer, J.A., Kang, H.K., Kaufmann, D.E., Kollmann, P., Krimigis, S.M., Kusnierkiewicz, D., Lauer, T.R., Lee, J.E., Lindstrom, K.L., Linscott, I.R., Lisse, C.M., Lunsford, A.W., Mallder, V.A., Martin, N., McComas, D.J., McNutt, R.L., Mehoke, D., Mehoke, T., Melin, E.D., Mutchler, M., Nelson, D., Nimmo, F., Nunez, J.I., Ocampo, A., Owen, W.M., Paetzold, M., Page, B., Parker, A.H., Parker, J.W., Pelletier, F., Peterson, J., Pinkine, N., Piquette, M., Porter, S.B., Protopapa, S., Redfern, J., Reitsema, H.J., Reuter, D.C., Roberts, J.H., Robbins, S.J., Rogers, G., Rose, D., Runyon, K., Retherford, K.D., Ryschkewitsch, M.G., Schenk, P., Schindhelm, E., Sepan, B., Showalter, M.R., Singer, K.N., Soluri, M., Stanbridge, D., Steffl, A.J., Strobel, D.F., Stryk, T., Summers, M.E., Szalay, J.R., Tapley, M., Taylor, A., Taylor, H., Throop, H.B., Tsang, C.C.C., Tyler, G.L., Umurhan, O.M., Verbiscer, A.J., Versteeg, M.H., Vincent, M., Webbert, R., Weidner, S., Weigle, G.E., White, O.L., Whittenburg, K., Williams, B.G., Williams, K., Williams, S., Woods, W.W., Zangari, A.M., Zirnstein, E., 2015. The pluto system: initial results from its exploration by new horizons. Science 350 292, 291–298.

Thomas, P.J., Schubert, G., 1987. Finite element models of non-Newtonian crater relaxation. J. Geophys. Res. 92 (B4), E749–E758. doi:10.1029/JB1092iB1004p1020E1749.

Thomas, P.J., Schubert, G., 1988. Power law rheology of ice and the relaxation style and retention of craters on Ganymede. J. Geophys. Res. 93 (B11), 13755–13762. doi:10.11029/JB13093iB13711p13755.

Thomas, P.J., Squyres, S.W., 1988. Relaxation of impact basins on icy satellites. J. Geophys. Res. 93, 14919–14932. doi:10.11029/JB14093iV14912p14919.

Tiedje, T., Mitchell, K.A., Lau, B., Ballestad, A., Nodwell, E., 2006. Radiation transport model for ablation hollows on snowfields. J. Geophys. Res. 111 (F2).

Trowbridge, A.J., Melosh, H.J., Steckloff, J.K., Freed, A.M., 2016. Vigorous convection as the explanation for Pluto's polygonal terrain. Nature 534 7605, 79–81. doi:10.1038/nature18016.

Umurhan, O.M. et al., 2016. HYPERLINK \l "S0019-1035(16)30526-7" This issue.

White, O.L., Umurhan, O.M., Moore, J.,M., Howard, A.D., 2015. Modeling of ice pinnacle formation on Callisto. J. Geophys. Res. Planets 121, 21–45. doi:10.1002/2015JE004846.

White, O.L., Moore, J.M., Stern, S.A., Weaver, H.A., Olkin, C.B., Ennico, K., Young, L.A., Cheng, A.F., the New Horizons Geology and Geophysics Imaging Theme Team, 2016. Geomorphological mapping of the encounter hemisphere on Pluto. Lunar Planet. Sci. XLVII abstr. 2479.

Yamashita, Y., Kato, M., Arakawa, M., 2010. Experimental study on the rheological properties of polycrystalline solid nitrogen and methane: implications for tectonic processes on triton. Icarus 207, 972–977.